The Center-to-Limb Behavior of Excess Solar UV Flux from Active Regions

Patrick Crane[1], Linton Floyd[2], John Cook[3], Lynn Herring[2], and Eugene Avrett[4]

[1]Code 7213, Remote Sensing Division Naval Research Laboratory, Washington, DC 20375 USA
[2]Interferometrics, 14120 Parke Long Court, Suite 103, Chantilly, VA 20151, USA
[3]Code 7668, E.O. Hulburt Center for Space Research, Naval Research Laboratory, Washington, DC 20375 USA
[4]Harvard-Smithsonian Center for Astrophysics, 60 Garden Street, Cambridge, MA 02138 USA

Abstract

The center-to-limb variation of solar radiant flux places important constraints on candidate models of the solar atmosphere. Time series of solar ultraviolet (UV) irradiances measured by the Solar Ultraviolet Spectral Irradiance Monitor (SUSIM) aboard the Upper Atmosphere Research Satellite (UARS) have been analyzed to describe the center-to -limb behavior of the excess surface brightness of solar active regions over the wavelength range 142–265 nm. From 27 September 1994 to 4 June 1995, solar UV irradiances in the 168–210 nm wavelength range exhibited strong 13.5-day periodicity, and weaker 13.5 day periodicity elsewhere. We show that, on average, active regions exhibit weak limb brightening for 142–168 nm, strong limb darkening for 168–210 nm, and weak limb darkening for 210–265 nm. In the shortest wavelength region, our results agree well with a different time series analysis of SOLSTICE irradiances by Worden, Woods and Bowman (WWB, 2001). However, the strong limb darkening found for active regions at intermediate wavelengths differed substantially from earlier quiet sun observations and those derived from the semi-empirical solar atmospheres model described by Fontenla et al. (1999), which included subsequent improvements by Avrett.

Overview

The solar UV spectral irradiance, the spectral sum of radiant flux over the solar disk, varies continuously. In the solar UV below 265 nm that we are considering here, these variations are the result of bright areas on the solar surface called *active regions*. These active regions grow and decay on time scales of weeks to months and their aggregate output is roughly synchronized with the solar activity cycle. The ∼27-day solar rotation is another source of consistent periodicity in the UV irradiances. As the sun rotates, the solar UV irradiance changes as active regions pass over the solar disk. Embedded within time series of the solar UV irradiances are their size, contrast, and center-to-limb variation. Accordingly, solar irradiance time series can give clues to solar atmospheric structure.

The ideal way to measure the center-to-limb dependence is to view the sun simultaneously from two different directions. Given that these measurements have not yet been made and are not currently planned at UV wavelengths, we seek to infer the center-to-limb dependence through analysis of UV irradiance time series. We analyze the SUSIM time series in the frequency domain, extending the Fourier analyses of previous investigators, especially, the work of Donnelly and his collaborators (Donnelly et al., 1982; Donnelly et al., 1986; Donnelly & Puga, 1990). In particular we analyze the wavelength-dependent amplitude ratios of ∼13.5-day and ∼27-day periodicities in the SUSIM UV irradiance data. Active region "two-sidedness" with respect to longitude and stronger limb darkening increase the value of the ratio.

The Data Analysis Model

In this section, we present a condensed version of our approach for translating the wavelength-dependent ratios of ∼13.5-day to ∼27-day amplitudes into physically meaningful quantities. The values of the ratios vary with time because the tendency for two-sidedness interacts with other factors including the longitudinal spread and evolution of active regions. Potentially, if that variability could be somehow "calibrated", as is done in other areas of astronomy that use Fourier analysis – radio, optical, and speckle interferometry – the two factors could be separated. In this analysis, our knowledge of the center-to-limb behaviors of the international sunspot number, R, and the solar radio flux density, $\mathsf{F}_{10.7cm}$, will provide the means to do so. Because limb darkening is weak for both indices, an episode of strong two-sidedness is optimal for this study. Such an episode of unusual ∼13.5-day variations occurred during the UARS mission from 27 September 1994 to 4 June 1995 (Floyd et al., 1997; Crane, 1998).

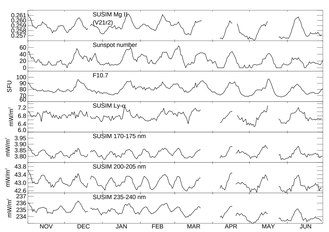

To this end, we have adopted a simple two-component model:

$$s_\lambda(t) = q_\lambda + c_\lambda i(t) \star f_\lambda(t), \tag{1}$$

where $s_\lambda(t)$ is the signal of interest at each wavelength; q and c are wavelength-dependent constants; $f(t)$ is a wavelength-dependent smoothing function; $i(t)$ is a wavelength-independent series of impulses (Dirac delta functions); and '$\star$' indicates convolution. The nth impulse in $i(t)$ represents an active region crossing the center of the solar disk at time t:

$$i(t) = \sum_n a_n \delta(t - t_n), \tag{2}$$

where the constants a_n and times t_n are independent of wavelength.
The signal contributed by the nth active region is

$$s_{\lambda,n}(t) = c_\lambda a_n f_\lambda(t - t_n). \tag{3}$$

In physical terms, s_λ is an observable such as an ultraviolet irradiance or the solar radio flux density at wavelength λ. If it is an irradiance, q_λ is the integrated irradiance of the underlying disk at wavelength λ which includes everything that does not contribute to the rotational variations. In the frequency domain, the Fourier transform, $S_\lambda(f)$, of the signal is given by

$$S_\lambda(f) = q_\lambda \delta(f) + c_\lambda I(f) F_\lambda(f), \tag{4}$$

where $\delta(f)$ is the Dirac delta function at zero frequency; $I(f)$, the Fourier transform of the series of impulses (Eq. 2); and $F_\lambda(f)$, the Fourier transform of the smoothing function.
The ratio of the ∼13.5-day and ∼27-day signal transforms is then:

$$\mathcal{R}_\lambda = S_\lambda(2/P_\odot)/S_\lambda(1/P_\odot). \tag{5}$$

where $P_\odot$ is the 27-day synodic solar rotation period. We separate this ratio into time- and wavelength-dependent terms, $\mathcal{I}$ and $\mathcal{F}_\lambda$, respectively:

$$\mathcal{R}_\lambda = \mathcal{I}\mathcal{F}_\lambda, \tag{6}$$

where the source and filter parameters, $\mathcal{I}$ and $\mathcal{F}_\lambda$, are given by

$$\mathcal{I} = I(2/P_\odot)/I(1/P_\odot), \tag{7}$$
$$\mathcal{F}_\lambda = F_\lambda(2/P_\odot)/F_\lambda(1/P_\odot). \tag{8}$$

The source parameter, $\mathcal{I}$, depends only upon the time interval analyzed and is a measure of the degree of two-sidedness. Its variation with time is responsible for the amplitude variations in $\mathcal{R}_\lambda$ reported by Donnelly & Puga (1990).
Time series analysis cannot detect the center-to-limb variation of the quiet disk. Instead, the center-to-limb variation of the excess irradiance of active regions is inferred. To this end, In Eq. 3, we associate

$$f_\lambda(t - t_n) = \mathcal{L}^*_\lambda(\mu_n) = \begin{cases} \mu L^*_\lambda(\mu_n), & 0 \le \mu \le 1, \\ 0, & \text{otherwise,} \end{cases} \tag{9}$$

$$c_\lambda = I^*_\lambda(1), \tag{10}$$

$$a_n = \Omega_n(1). \tag{11}$$

where $\mathcal{L}^*_\lambda(\mu_n)$ and $L^*_\lambda(\mu)$ are the center-to-limb coefficients of the excess irradiance and surface brightness, respectively, associated with the nth active region. We use two functional forms to describe the center-to-limb behavior.

- The form used to describe limb brightening by WWB gives in this case:

$$\mathcal{L}^*_\lambda(\mu) = \begin{cases} \mu \max[\mathsf{R_c} + 2(1 - \mathsf{R_c})(\mu - \mu^2/2), 0], & 0 \le \mu \le 1, \\ 0, & \text{otherwise.} \end{cases} \tag{12}$$

where $\mathsf{R_c}$ is the surface-brightness ratio. (The maximum function is used to avoid negative values when $\mathsf{R_c} < 0$.)

- The description of limb darkening by Hestroffer (1997) and Hestroffer & Magnan (1998), uses a truncated power law in μ characterized by the exponent, x:

$$\mathcal{L}^*_\lambda(\mu) = \begin{cases} \mu^x, & 0 \le \mu \le 1, \\ 0, & \text{otherwise.} \end{cases} \tag{13}$$

Center-to-Limb Variation Classification

The figure below displays the two model smoothing functions for $\mathsf{R_c}$ and μ^x assuming $P_\odot = 27$ days. The constant curves are identical ($\mathsf{R_c} = 1$, $x = 1$, $\mathcal{F}_\lambda = 0.424$) and the other two pairs have the same filter parameter ($\mathsf{R_c} = -19.4$, $x = 8.37$, $\mathcal{F}_\lambda = 0.85$ and $\mathsf{R_c} = 7.4$, $x = 0$, $\mathcal{F}_\lambda = 0$). The relationships between $\mathcal{F}_\lambda$ and $\mathsf{R_c}$, and $\mathcal{F}_\lambda$ and x, are shown in the middle and bottom panels.

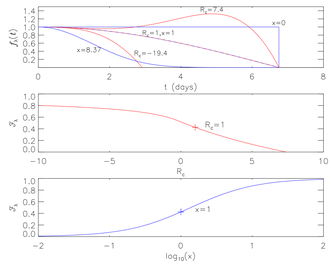

The table below displays the correspondence between filter parameter, $\mathcal{F}_\lambda$, the center-to-limb model parameters for each functional form, and the FWHM of T for μ^x, again assuming $P_\odot = 27$ days.

$\mathcal{F}_\lambda$	$\mathsf{R_c}$	x	T(dy)	Classification
0.000	7.40	0.00	13.50	Very strong limb brightening
0.110	5.36	0.16	13.40	Strong limb brightening
0.220	3.63	0.37	12.20	Medium limb brightening
0.330	2.13	0.66	10.40	Weak limb brightening
0.424	1.00	1.00	9.00	Constant surface brightness
0.550	-0.33	1.72	7.27	Weak limb darkening
0.700	-3.21	3.39	5.36	Medium limb darkening
0.850	-19.41	8.37	3.46	Strong limb darkening
1.000	∞	∞	0.00	Very strong limb darkening

Calibration with $\mathsf{F}_{10.7cm}$ and Sunspot Number

If the ratio, $\mathcal{R}_\lambda$, and filter parameter, $\mathcal{F}_\lambda$, are known, the source parameter, $\mathcal{I}$, is easily derived. In the episode under study, the ratios, $\mathcal{R}_\lambda$, are known for two common solar indices – the international sunspot number, R, and the solar radio flux density, $\mathsf{F}_{10.7cm}$ (Crane, 1998). The smoothing functions, $f_\lambda(t)$, and the filter parameters, $\mathcal{F}_\lambda$, are known empirically for both indices. Therefore, as illustrated in the following table, two independent values of the source parameter, $\mathcal{I}$, can be derived and combined to produce a weighted average, which in turn calibrates Eq. 6 during this episode.
It is then straightforward to obtain the filter parameters, $\mathcal{F}_\lambda$, from the measured ratios, $\mathcal{R}_\lambda$, at ultraviolet wavelengths.

Index	$f_\lambda(t)$	T	$\mathcal{F}_\lambda$	$\mathcal{R}_\lambda$	$\mathcal{I}$
R	cubic spline	10.3	0.380	1.20 ±0.09	3.15 ±0.23
$\mathsf{F}_{10.7cm}$	truncated Gaussian	11.1	0.158	0.48 ±0.04	3.01 ±0.27
Weighted mean ($\mathcal{I}$)	—	—	—	—	3.10 ±0.07

The time interval chosen for study extends from 27 September 1994 to 4 June 1995 which was during the declining phase of solar cycle 22. Reproduced in the figure below are the time series and clean Fourier transforms (the latter as a function of period P) (Crane, 1998) for international sunspot number, R, and for the solar radio flux density, $\mathsf{F}_{10.7cm}$. The salient differences in the considered time series should be noted.

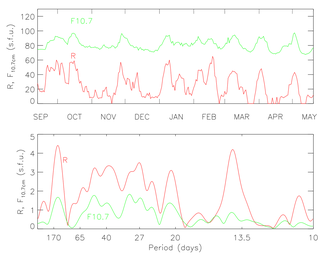

Analysis of SUSIM UV Irradiance Data

The (UARS days 1112–1362) V19 Level-3BS 1-nm gridded, 1-nm integrated ultraviolet irradiances measured by the SUSIM were analyzed by the DFT/CLEAN technique used by Crane (1998), which combines the direct Fourier transform (DFT) and the CLEAN deconvolution algorithm. The amplitudes of the clean Fourier transforms as a function of period and wavelength for the 27 September 1994 to 4 June 1995 time period are shown in the gray-scale contour plot below.

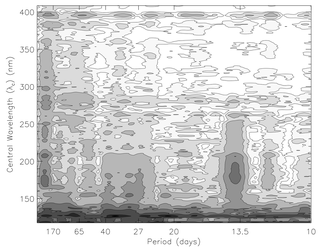

The ordinate is the central wavelength, λ_c, of the 5-nm windows, and the abscissa is the period, P. The values at each wavelength are normalized to the corresponding DC value at zero frequency. The grey-scale and contour levels correspond to (0.005,0.01,0.02,0.05,0.1,0.2,0.5,0.9) of the peak normalized value of 4.44.
Because the solar irradiances at these wavelengths vary by about five orders of magnitude, the Fourier transform at each wavelength has been normalized by its "DC" value. To reduce the noise in the contour plot, the normalized amplitudes have been smoothed in wavelength with a 5-nm boxcar. While other periodicities are visible, those of interest at ∼27 days and ∼13.5 days are significant in the wavelength interval 142–265 nm. Individual analyses were also performed for the SUSIM Ly-α and core-to-wing Mg II indices.
The figure below displays normalized peak amplitudes in two windows, covering periods of 25–30 days (∼27 day) and 12.5–15.0 days (∼13.5 day), in the normalized CLEAN Fourier transform at each wavelength (142–265 nm).

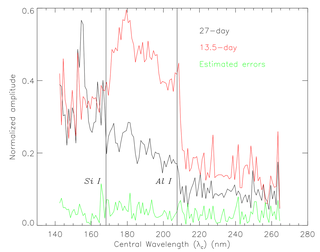

The abscissa is the central wavelength, λ_c, of the 1-nm bins. Vertical lines indicate the Si I edge at 168.2 nm and the Al I edge at 207.6 nm. The estimated errors are also plotted.
Three regions are easily distinguished, separated by the Si I edge at 168.2 nm and by the Al I edge at 207.6 nm. In the region below the Si I edge, the amplitudes of the ∼27-day and ∼13.5-day periodicities are approximately constant and equal. In the region above the Al I edge, the amplitudes of the ∼27-day and ∼13.5-day periodicities are approximately constant and the latter are twice the former. Between the Si I and Al I edges the amplitudes of the ∼27-day periodicities decline approximately linearly from the values at the short wavelengths to those at the long wavelengths. On the other hand, the amplitudes of the ∼13.5-day periodicities increase by about a factor of 2 across the Si I edge and decrease by about a factor of 1.5 across the Al I edge.

The ratios, $\mathcal{R}_\lambda$, are readily calculated from these measurements. Displayed below are the filter parameters, $\mathcal{F}_\lambda$, calculated by dividing the ratios, $\mathcal{R}_\lambda$, by the weighted mean source parameter, $\langle\mathcal{I}\rangle$, which, in turn, was calculated earlier from sunspot number, R, and the solar radio flux density, $\mathsf{F}_{10.7cm}$. Also shown are the theoretical filter parameters for R, $\mathsf{F}_{10.7cm}$, the measured values for the SUSIM Ly-α irradiance, and the Mg II core-to-wing ratio index.

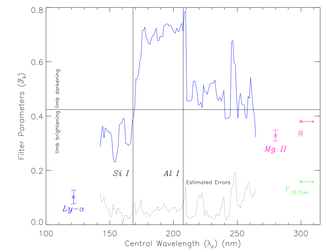

Vertical lines indicate the Si I edge at 168.2 nm and the Al I edge at 207.6 nm. The dotted line indicates the estimated errors derived from the errors in the amplitudes.
Not surprisingly, the behaviors of $\mathcal{F}_\lambda$ and $\mathcal{R}_\lambda$ are similar in that there are abrupt changes near to the Al I and Si I edges. The table below shows the averages of $\mathcal{F}_\lambda$ for the three wavelength regions, Ly-α, and for the Mg II index. Most notable is the strong limb darkening for 175–210 nm. A separate analysis indicates that instrumental rather than solar effects are dominant in the Ly-α result.

λλ (nm)	$\langle\mathcal{R}_\lambda\rangle$	$\langle\mathcal{F}_\lambda\rangle$	Classification	$\mathsf{R_c}$	x	T(dy)
Ly-α	0.32±0.08	0.102±0.025	Very strong limb brightening	5.50	0.15	13.4
142–168	1.09±0.18	0.352±0.060	Weak limb brightening	1.85	0.73	10.1
175–210	2.20±0.18	0.710±0.060	Strong limb darkening	-3.58	3.56	5.2
210–265	1.39±0.23	0.448±0.073	Weak limb darkening	0.74	1.12	8.7
Mg II	1.02±0.06	0.328±0.020	Medium limb brightening	2.16	0.66	10.5

The average values of the filter parameters have been used for classification and to derive values of $\mathsf{R_c}$, x, and T.

Measurement Comparisons

Displayed below are the active region surface brightness ratios for 140–175 nm derived from the filter parameters from the SUSIM 1-nm ratios, the SOLSTICE plage continuum and emission lines (solid circles) from WWB, and quiet sun measurements from Brekke & Kjeldseth-Moe (1994) and from Samain (1979).

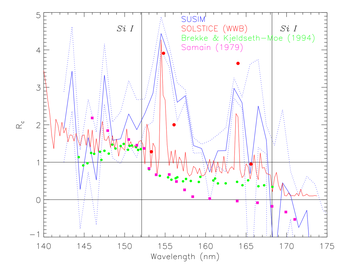

The dotted lines indicate the estimated errors in the SUSIM ratios. The spectral features are broader for SUSIM than for SOLSTICE because of SUSIM's lower spectral resolution.

The exponents, x, for the wavelength range 165–270 nm derived from the filter parameters for the SUSIM 5-nm smoothed ratios are displayed below. We display x rather than $\mathsf{R_c}$ because limb darkening dominates above 168 nm. The dotted line represents the estimated errors in the SUSIM exponents. Exponents were derived from Samain (1979), Kjeldseth-Moe & Milone (1978), and Bonnet (1968) for quiet-disk continuum. Over the wavelength range 175–210 nm, the average difference in exponent between the SUSIM and Samain results is 1.83±0.08.

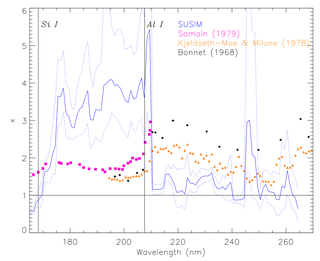

Active regions exhibit a gradual transition to strong limb darkening extending from the Si I edge at 168.2 nm to about 175 nm. The transition back to weak limb darkening occurs abruptly at 210 nm. Between these limits, the active regions and the quiet-disk continuum (Samain 1979; Kjeldseth Moe & Milone, 1978; Bonnet 1968) exhibit approximately constant strong and weak limb darkening, respectively. Above the Al I edge at 207.6 nm, Kjeldseth Moe & Milone (1978) and Bonnet (1968) show weak or medium limb darkening for the quiet-disk continuum. The following table presents comparisons between the mean filter parameters, $\langle\mathcal{F}_\lambda\rangle$, found by SUSIM and the corresponding filter parameters for the quiet sun, $\langle\mathcal{F}_\lambda^{quiet}\rangle$, as determined from earlier measurements.

λλ (nm)	$\langle\mathcal{F}_\lambda\rangle$	$\langle\mathcal{F}_\lambda^{model}\rangle$	$\langle\mathcal{F}_\lambda^{model,QS}\rangle$	$\langle\mathcal{F}_\lambda^{model,FP}\rangle$	$\langle\mathcal{F}_\lambda^{quiet}\rangle$
142–168	0.352±0.060	0.372±0.020	0.402±0.033	0.379±0.018	0.435±0.036[b] 0.444±0.065[c]
175–210	0.710±0.060	0.486±0.088[a]	0.530±0.054	0.516±0.042	0.577±0.037[c]
210–265	0.448±0.073	0.471±0.104	0.522±0.044	0.514±0.048	0.536±0.033[d] 0.642±0.023[e]

[a] excluding two outliers.
[b] Brekke & Kjeldseth-Moe (1994)
[c] Samain (1979)
[d] Kjeldseth Moe & Milone (1978)
[e] Bonnet (1968)

Semi-Empirical Model Comparison

We also compared the SUSIM results for 142–265 nm with calculations based on the semi-empirical model atmospheres (Fontenla et al., 1999) with modifications by Avrett as depicted in the figure below.

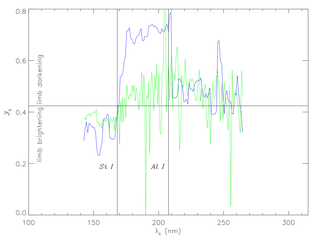

Excess irradiances were calculated by taking the difference between the faint plage and quiet sun model atmospheres. There is general agreement between the model ($\mathcal{F}_\lambda^{model}$) and SUSIM-derived ($\mathcal{F}_\lambda$) center-to-limb parameters for wavelengths 142–175 nm and 210–263 nm. However, much stronger limb darkening is observed for 175–210 nm than is obtained using the semi-empirical model. Additionally, the table above also includes separate entries for the QS ($\mathcal{F}_\lambda^{model,QS}$) and FP ($\mathcal{F}_\lambda^{model,FP}$) models and for the measured quiet sun ($\mathcal{F}_\lambda^{quiet}$).

Summary and Conclusions

We have analyzed the SUSIM UV irradiance time series for the time period 27 September 1994 to 4 June 1995 to determine the center-to-limb variation of solar UV radiant flux from active regions. The locations of active regions during this period are reflected in the source parameter, $\mathcal{I}$, which is determined by analyzing sunspot number (R) and $\mathsf{F}_{10.7cm}$ radio flux time series. The center-to-limb behavior is characterized by a filter parameter, $\mathcal{F}_\lambda$, which is calculated from the amplitude ratio of ∼13.5-day and ∼27-day periodicities.
Our principal conclusions are:

- The solar center-to-limb variation is divided into three wavelength regimes:
  - 142–168 nm: Weak Limb Brightening
  - 175–210 nm: Strong Limb Darkening
  - 210–265 nm: Weak Limb Darkening
- SUSIM center-to-limb results agree with that WWB derived from the SOLSTICE irradiance time series for the wavelength range 142–168 nm.
- SUSIM center-to-limb results are in general agreement with measurement results derived for the quiet sun in the 142–168 nm and 210–265 nm wavelength ranges; SUSIM results show somewhat more brightening in the former and somewhat less darkening in the latter, especially near the Al edge.
- SUSIM center-to-limb results are in general agreement with measurement results derived from semi-empirical model atmospheres (Fontenla et al., 1999) in the 142–168 nm and 210–265 nm wavelength ranges.
- SUSIM center-to-limb results show far greater limb darkening than do those derived from quiet sun measurements and those derived from the semi-empirical model in the 175–210 nm wavelength range.

The difference in the center-to-limb variation found for 175–210 nm is by no means a subtle effect. Rather, this difference is quite substantial. If borne out by further studies, this has major implications for our understanding of the structure of the solar atmosphere. Direct solar UV radiance (i.e. imaging) measurements are needed to perhaps confirm and extend this result.

Bibliography

Bonnet, R. (1968). Recherches sur l'émission continue du Soelil entre 1950 &Aring et 3000 Å. *Annales d'Astrophysique*, 31:597–+.

Brekke, P. and Kjeldseth-Moe, O. (1994). The solar UV continuum 1440-1680 and its center-to-limb variation. *Sol. Phys.*, 150:19–47.

Brueckner, G. E., Edlow, K. L., Floyd, L. E., Lean, J. L., and Vanhoosier, M. E. (1993). The solar ultraviolet spectral irradiance monitor (SUSIM) experiment on board the Upper Atmosphere Research Satellite (UARS). *J. Geophys. Res.*, 98:10695–+.

Crane, P. C. (1998). Two Unusual Episodes of ∼13-Day Variations. *Sol. Phys.*, 177:243–253.

Crane, P. C. (2001). Applications of the DFT/CLEAN Technique to Solar Time Series. *Sol. Phys.*, 203:381–408.

Donnelly, R. F., Heath, D. F., and Lean, J. L. (1982). Active-region evolution and solar rotation variations in solar UV irradiance, total solar irradiance, and soft X rays. *J. Geophys. Res.*, 87:10318–10324.

Donnelly, R. F., Hinteregger, H. E., and Heath, D. F. (1986). Temporal variations of solar EUV, UV, and 10,830-A radiations. *J. Geophys. Res.*, 91:5567–5578.

Donnelly, R. F. and Puga, L. C. (1990). Thirteen-day periodicity and the center-to-limb dependence of UV, EUV, and X-ray emission of solar activity. *Sol. Phys.*, 130:369–390.

Floyd, L., Brueckner, G., Crane, P., Prinz, D., and Herring, L. (1997). Correlations of Solar Cycle 22 UV Irradiance. In *ESA SP-415: Correlated Phenomena at the Sun, in the Heliosphere and in Geospace*, pages 235–+.

Fontenla, J., White, O. R., Fox, P. A., Avrett, E. H., and Kurucz, R. L. (1999). Calculation of Solar Irradiances. I. Synthesis of the Solar Spectrum. *ApJ*, 518:480–499.

Hestroffer, D. (1997). Centre to limb darkening of stars. New model and application to stellar interferometry. *A&A*, 327:199–206.

Hestroffer, D. and Magnan, C. (1998). Wavelength dependency of the Solar limb darkening. *A&A*, 333:338–342.

Kjeldseth Moe, O. and Milone, E. F. (1978). Limb darkening 1945-3245 A for the quiet sun from SKYLAB data. *ApJ*, 226:301–314.

Samain, D. (1979). Solar continuum data on absolute intensities, center to limb variations and Laplace inversion between 1400 and 2100 A. *A&A*, 74:225–228.

Woods, T. N., Rottman, G. J., and Ucker, G. J. (1993). Solar-Stellar Irradiance Comparison Experiment 1. II - Instrument calibrations. *J. Geophys. Res.*, 98:10679–+.

Worden, J. R., Woods, T. N., and Bowman, K. W. (2001). Far-Ultraviolet Intensities and Center-to-Limb Variations of Active Regions and Quiet Sun Using UARS SOLSTICE Irradiance Measurements and Ground-based Spectroheliograms. *ApJ*, 560:1020–1034.